

Cite as: T. Song *et al.*, *Science*
10.1126/science.aar4851 (2018).

Giant tunneling magnetoresistance in spin-filter van der Waals heterostructures

Tiancheng Song,^{1*} Xinghan Cai,^{1*} Matisse Wei-Yuan Tu,² Xiaoou Zhang,³ Bevin Huang,¹ Nathan P. Wilson,¹ Kyle L. Seyler,¹ Lin Zhu,⁴ Takashi Taniguchi,⁵ Kenji Watanabe,⁵ Michael A. McGuire,⁶ David H. Cobden,¹ Di Xiao,^{3†} Wang Yao,^{2†} Xiaodong Xu^{1,4†}

¹Department of Physics, University of Washington, Seattle, Washington 98195, USA. ²Department of Physics and Center of Theoretical and Computational Physics, University of Hong Kong, Hong Kong, China. ³Department of Physics, Carnegie Mellon University, Pittsburgh, PA 15213, USA. ⁴Department of Materials Science and Engineering, University of Washington, Seattle, WA 98195, USA. ⁵National Institute for Materials Science, Tsukuba, Ibaraki 305-0044, Japan. ⁶Materials Science and Technology Division, Oak Ridge National Laboratory, Oak Ridge, TN 37831, USA.

*These authors contributed equally to this work.

†Corresponding author. Email: xuxd@uw.edu (X.X.); wangyao@hku.hk (W.Y.); dixiao@cmu.edu (D.X.)

Magnetic multilayer devices that exploit magnetoresistance are the backbone of magnetic sensing and data storage technologies. Here, we report multiple-spin-filter magnetic tunnel junctions (sf-MTJs) based on van der Waals (vdW) heterostructures in which atomically thin chromium triiodide (CrI₃) acts as a spin-filter tunnel barrier sandwiched between graphene contacts. We demonstrate tunneling magnetoresistance which is drastically enhanced with increasing CrI₃ layer thickness, reaching a record 19,000% for magnetic multilayer structures using four-layer sf-MTJs at low temperatures. Using magnetic circular dichroism measurements, we attribute these effects to the intrinsic layer-by-layer antiferromagnetic ordering of the atomically thin CrI₃. Our work reveals the possibility to push magnetic information storage to the atomically thin limit and highlights CrI₃ as a superlative magnetic tunnel barrier for vdW heterostructure spintronic devices.

Many two-dimensional (2D) materials can be incorporated into artificial heterostructures without the need for lattice matching. These materials thus provide a unique platform for exploring emerging phenomena and device function at the designed atomic interfaces (1, 2). However, magnetic memory and processing applications were out of reach in van der Waals (vdW) heterostructures before the recent discovery of suitable 2D magnetic materials (3–10). One of these is the magnetic insulator chromium triiodide (CrI₃), which in bilayer form has been found to possess a layered-antiferromagnetic ground state. Magneto-optical Kerr effect (MOKE) measurements suggest that the spins align ferromagnetically out-of-plane within each layer but antiferromagnetically between layers, resulting in vanishing net magnetization (Fig. 1A, left) (3).

This layered-antiferromagnetic ordering makes CrI₃ desirable for realizing atomically thin magnetic multilayer devices. When the magnetizations of the two layers in a bilayer are switched between anti-parallel (Fig. 1A, left) and parallel states (Fig. 1A, middle and right), giant tunneling magnetoresistance (TMR) is produced by the double spin-filtering effect (11, 12). In general, spin filters, which create and control spin-polarized currents, are the fundamental element in magnetic multilayer devices, such as spin valves (13–15), magnetic tunnel junctions (MTJs) (16–21) and double spin-filter MTJs

(sf-MTJs) (11, 12). Compared with the existing magnetic multilayer devices that require different choices of (metallic or insulating) magnets and spacers, the layered-antiferromagnetic structure in bilayer CrI₃ avoids the need for fabricating separate spin filters with spacers. This guarantees sharp atomic interfaces between spin filters, crucial for achieving large sf-TMR.

An even more intriguing possibility arises if the intrinsic layered-antiferromagnetic structure of CrI₃ extends beyond the bilayer. In this case, every layer should act as another spin filter oppositely aligned in series, greatly enhancing the sf-TMR as the number of layers increases. The associated multiple magnetic states may also enable multiple magnetoresistance states for potentially encoding information in an individual sf-MTJ device. Moreover, being insulators, atomically thin CrI₃ single crystals can be integrated into vdW heterostructures as tunnel barriers in place of non-magnetic dielectrics, such as hexagonal boron nitride (hBN) (22, 23) or transition metal dichalcogenides (24), adding magnetic switching functionality. The realization of such vdW heterostructure sf-MTJs could produce novel 2D magnetic interface phenomena (25) and enable spintronics components such as spin current sources and magnetoresistive random-access memory (MRAM) (26).

Here, we demonstrate vdW-engineered sf-MTJs based on atomically thin CrI₃ with extraordinarily large sf-TMR. Figure

1B shows the essential structure of the sf-MTJ, which consists of two few-layer graphene contacts separated by a thin CrI₃ tunnel barrier. The sf-MTJ is sandwiched between two hexagonal boron nitride (hBN) flakes to avoid degradation. We have made and investigated devices with bilayer, trilayer, and four-layer CrI₃. All measurements were carried out at a temperature of 2 K, unless otherwise specified.

We begin with the case of bilayer CrI₃. The inset of Fig. 1C is an optical micrograph of a device with the structure illustrated in Fig. 1B, obtained by stacking exfoliated 2D materials using a dry transfer process in a glovebox (27). The tunneling junction area is less than $\sim 1 \mu\text{m}^2$ to avoid effects caused by lateral magnetic domain structures (3, 4). Figure 1C shows the tunneling current (I_t) as a function of DC bias voltage (V) at selected magnetic fields ($\mu_0 H$) (27). Unlike in tunneling devices using non-magnetic hBN as the barrier (22, 23), it has a strong magnetic field dependence. As shown in Fig. 1C, I_t is much smaller at $\mu_0 H = 0$ T (purple trace) than it is in the presence of an out-of-plane field ($\mu_0 H_{\perp}$, red trace) or an in-plane field ($\mu_0 H_{\parallel}$, green trace). This magnetic-field-dependent tunneling current implies a spin-dependent tunneling probability related to the field-dependent magnetic structure of bilayer CrI₃.

To investigate the connection between the bilayer CrI₃ magnetic states and the magnetoresistance, we measured I_t as a function of $\mu_0 H_{\perp}$ at a particular bias voltage (-290 mV). The green and orange curves in Fig. 2A correspond to decreasing and increasing magnetic fields, respectively. I_t exhibits plateaus with two values, about -36 nA and -155 nA. The lower plateau is seen at low fields, and there is a sharp jump to the higher plateau when the magnetic field exceeds a critical value. We also employed reflective magnetic circular dichroism (RMCD) to probe the out-of-plane magnetization of the bilayer CrI₃ near the tunneling area. Figure 2B shows the RMCD signal as a function of $\mu_0 H_{\perp}$ under similar experimental conditions to the magnetoresistance measurements (27). The signal is small at low fields, corresponding to a layered-antiferromagnetic ground state ($\uparrow\downarrow$ or $\downarrow\uparrow$), where the arrows indicate the out-of-plane magnetizations in the top and bottom layers respectively. As the magnitude of the field increases there is a step up to a larger signal corresponding to the fully spin-polarized states ($\uparrow\uparrow$ and $\downarrow\downarrow$), consistent with earlier MOKE measurements on bilayer CrI₃ (3). Additional bilayer device measurements can be found in (27).

A direct comparison of I_t and RMCD measurements provides the following explanation of the giant sf-TMR: in the $\uparrow\downarrow$ or $\downarrow\uparrow$ states at low field the current is small because spin-conserving tunneling of an electron through the two layers in sequence is suppressed. The step in I_t occurs when the magnetic field drives the bilayer into the $\uparrow\uparrow$ and $\downarrow\downarrow$ states and this suppression is removed. This is known as the double spin-filtering effect (11, 12), and it can be modeled by treating

the two monolayers as tunnel-coupled spin-dependent quantum wells (27).

We quantify the sf-TMR by $(R_{\text{ap}} - R_{\text{p}})/R_{\text{p}}$, where R_{ap} and R_{p} are the DC resistances with anti-parallel and parallel spin alignment in bilayer CrI₃ respectively, measured at a given bias. Figure 2C shows the value of this quantity as a function of bias extracted from the I_t - V curves in Fig. 1C. The highest sf-TMR achieved is 310% for magnetization fully aligned perpendicular to the plane and 530% for parallel alignment. The sf-TMR decreases as temperature increases and vanishes above the critical temperature at about 45 K (27).

The fact that the sf-TMR for in-plane magnetization is larger than for out-of-plane implies anisotropic magnetoresistance, which is a common feature in ferromagnets (28) and is a sign of anisotropic spin-orbit coupling stemming from the layered structure of CrI₃. The sf-TMR is also peaked at a certain bias and asymmetric between positive and negative bias. These observations are similar to the reported double sf-MTJs based on EuS thin films, where the asymmetry is caused by the different thickness and coercive fields of the two EuS spin-filters (12). Likewise, our data imply that the device lacks up-down symmetry, possibly because the few-layer graphene contacts are not identical in thickness. This broken symmetry also manifests as tilting of the current plateaus (Fig. 2A) and the finite nonzero RMCD value (Fig. 2B) in the layered-antiferromagnetic states (27).

To further investigate magnetic anisotropy and the assignment of magnetic states in the bilayer, we measured I_t as a function of in-plane magnetic field. As shown in Fig. 2D (black curve), I_t is smallest at zero field, in the layered-antiferromagnetic state, and smoothly increases with the magnitude of the field. This behavior has a natural interpretation in terms of a spin-canting effect. Once the magnitude of $\mu_0 H_{\parallel}$ exceeds about 4 T, the spins are completely aligned with the in-plane field and I_t saturates. Simulations of the canting effect to match the data (dashed purple curve) yield a magnetic anisotropy field of 3.8 T (27), much larger than the out-of-plane critical magnetic field of ± 0.6 T seen in Fig. 2A. These results therefore both demonstrate and quantify a large out-of-plane magnetic anisotropy in bilayer CrI₃.

We next consider the trilayer case. Figure 3, A and B, show I_t and RMCD, respectively, for a trilayer CrI₃ sf-MTJ as a function of out-of-plane field. There are four plateaus in the RMCD signal, at -14% , -5% , 5% , and 15% , the ratio between which is close to $-3:-1:1:3$. By analogy with the analysis of the $\uparrow\downarrow$ and $\downarrow\uparrow$ layered-antiferromagnetic states in the bilayer, we identify the trilayer ground state as $\uparrow\downarrow\uparrow$ or $\downarrow\uparrow\downarrow$ at zero field. We conclude that the interlayer coupling in trilayer CrI₃ is also antiferromagnetic, and the net magnetization in the ground state, and thus the RMCD value, is 1/3 of the saturated magnetization when the applied field fully aligns the three layers (27). The jumps in I_t and RMCD in Fig. 3, A and

B, are caused by the magnetization of an individual layer flipping, similar to what is seen in metallic layered-antiferromagnets (29–32).

We deduce that the low current plateau at small fields in Fig. 3A occurs because the two layered-antiferromagnetic states ($\uparrow\downarrow\uparrow$ and $\downarrow\uparrow\downarrow$) of the trilayer function as three oppositely polarized spin filters in series. Large enough fields drive the trilayer into fully spin-polarized states, which enhances tunneling and gives the high current plateaus. Figure 3C shows the sf-TMR as a function of bias derived from the I_t - V curves shown in the inset. The peak values are about 2,000% and 3,200% for magnetization fully aligned perpendicular and parallel to the plane, respectively, revealing a drastically enhanced sf-TMR compared to bilayer devices.

Increasing the CrI₃ thickness beyond three layers unlocks more complicated magnetic configurations. Figure 4, A and B, shows I_t and RMCD, respectively, for a four-layer device. There are multiple plateaus in each, signifying several magnetic configurations with different effects on the tunneling resistance. The small RMCD signal at low fields, below ~ 0.8 T, corresponds to the fully antiferromagnetic ground state, either $\uparrow\downarrow\uparrow\downarrow$ or $\downarrow\uparrow\downarrow\uparrow$. The fact that the RMCD is not zero (Fig. 4B) can be attributed to the asymmetry of the layers caused by the fabrication process, as in the bilayer case above (27). As expected, these fully antiferromagnetic states are very effective at suppressing the tunneling current since they act as four oppositely polarized spin filters in series, explaining the very low current plateau at small fields in Fig. 4A. Applying a large enough field fully aligns the magnetizations of all the layers ($\uparrow\uparrow\uparrow\uparrow$ or $\downarrow\downarrow\downarrow\downarrow$), producing the highest plateaus in both I_t and RMCD. Figure 4C shows the sf-TMR as a function of bias extracted from the I_t - V curves in the inset. The peak values are now about 8,600% and 19,000% for perpendicular and parallel field, respectively, representing a further enhancement of the sf-TMR compared to bilayer and trilayer cases.

The RMCD of four-layer CrI₃ also shows intermediate plateaus at about half the values in the fully aligned states (Fig. 4, B and F, and fig. S10), corresponding to magnetic states with half the net magnetization of the fully aligned states. There are four possible magnetic states for the positive field plateau: M_+ { $\uparrow\downarrow\uparrow\uparrow$, $\uparrow\uparrow\downarrow\uparrow$, $\downarrow\uparrow\uparrow\uparrow$, $\uparrow\uparrow\uparrow\downarrow$ }, the four time-reversal copies (M_-) being the negative field counterparts (Fig. 4D). The resulting spin filter configuration should then correspond to one layer polarized opposite to the other three.

Remarkably, in the range of fields where these 1:3 configurations occur the tunneling current displays multiple plateaus. The green curve in Fig. 4A shows three distinct intermediate I_t plateaus. Two are in the positive field corresponding to the same intermediate +18% RMCD plateau, and one is in the negative field range. The orange curve, sweeping in the opposite direction, is the time-reversal copy of the

green one. The possibility of lateral domains with different net magnetizations being the cause of these extra plateaus is inconsistent with field-dependent RMCD maps of all three measured four-layer CrI₃ sf-MTJs, none of which showed appreciable domains (27). In addition, the tunnel junction area is quite small compared with the typical domain size of a few microns in CrI₃ (3, 4).

Instead, these current plateaus probably originate from distinct magnetic states. Whereas the four states in M_+ are indistinguishable in RMCD because of the same net magnetization, the tunneling current is likely to be sensitive to the position of the one layer with minority magnetization. First, the $\downarrow\uparrow\uparrow\uparrow$ and $\uparrow\uparrow\downarrow\uparrow$ have only one current-blocking interface whereas $\uparrow\downarrow\uparrow\uparrow$ and $\uparrow\uparrow\uparrow\downarrow$ have two (green lines between adjacent layers with opposite magnetizations shown in Fig. 4D). Second, the current flow direction as well as the possibly asymmetric few-layer graphene contacts may introduce distinct sf-TMR either between the $\uparrow\downarrow\uparrow\uparrow$ and $\uparrow\uparrow\downarrow\uparrow$ states or between the $\downarrow\uparrow\uparrow\uparrow$ and $\uparrow\uparrow\uparrow\downarrow$ states (27). This asymmetry may also help to stabilize $\downarrow\uparrow\uparrow\uparrow$ and $\uparrow\uparrow\uparrow\downarrow$, which in general have higher energy than $\uparrow\downarrow\uparrow\uparrow$ and $\uparrow\uparrow\downarrow\uparrow$ in fully symmetric four-layer CrI₃. However, to identify the specific magnetic states corresponding to the current plateaus will require a means to distinguish the magnetization of individual layers (27).

The four-layer CrI₃ sf-MTJ points to the potential for using layered antiferromagnets for engineering multiple magnetoresistance states in an individual sf-MTJ. Figure 4, E and F, and fig. S10 show I_t and RMCD for two other four-layer CrI₃ sf-MTJs. They exhibit one or two intermediate plateaus, rather than the three observed in Fig. 4A. The sample dependence suggests that these intermediate states are sensitive to the environment of the CrI₃, such as the details of the contacts, implying potential tunability, for example by electrostatically doping the graphene contacts. One exciting future direction could be to seek electrically controlled switching between several different magnetoresistance states. Already the sf-TMR of up to 19,000% observed in four-layer devices is an order of magnitude larger than that of MgO-based conventional MTJs (19–21), and several orders of magnitude larger than achieved with existing sf-MTJs under similar experimental conditions (12). Although the demonstrated vdW sf-MTJs only work at low temperatures, these results highlight the potential of 2D magnets and their heterostructures for engineering novel spintronic devices with unrivaled performance (33, 34).

REFERENCES AND NOTES

1. A. K. Geim, I. V. Grigorieva, Van der Waals heterostructures. *Nature* **499**, 419–425 (2013). doi:10.1038/nature12385 Medline
2. K. S. Novoselov, A. Mishchenko, A. Carvalho, A. H. Castro Neto, 2D materials and van der Waals heterostructures. *Science* **353**, aac9439 (2016). doi:10.1126/science.aac9439 Medline
3. B. Huang, G. Clark, E. Navarro-Moratalla, D. R. Klein, R. Cheng, K. L. Seyler, D.

- Zhong, E. Schmidgall, M. A. McGuire, D. H. Cobden, W. Yao, D. Xiao, P. Jarillo-Herrero, X. Xu, Layer-dependent ferromagnetism in a van der Waals crystal down to the monolayer limit. *Nature* **546**, 270–273 (2017). [doi:10.1038/nature22391](https://doi.org/10.1038/nature22391) [Medline](#)
4. D. Zhong, K. L. Seyler, X. Linpeng, R. Cheng, N. Sivasdas, B. Huang, E. Schmidgall, T. Taniguchi, K. Watanabe, M. A. McGuire, W. Yao, D. Xiao, K. C. Fu, X. Xu, Van der Waals engineering of ferromagnetic semiconductor heterostructures for spin and valleytronics. *Sci. Adv.* **3**, e1603113 (2017). [doi:10.1126/sciadv.1603113](https://doi.org/10.1126/sciadv.1603113) [Medline](#)
 5. C. Gong, L. Li, Z. Li, H. Ji, A. Stern, Y. Xia, T. Cao, W. Bao, C. Wang, Y. Wang, Z. Q. Qiu, R. J. Cava, S. G. Louie, J. Xia, X. Zhang, Discovery of intrinsic ferromagnetism in two-dimensional van der Waals crystals. *Nature* **546**, 265–269 (2017). [doi:10.1038/nature22060](https://doi.org/10.1038/nature22060) [Medline](#)
 6. M. A. McGuire, H. Dixit, V. R. Cooper, B. C. Sales, Coupling of crystal structure and magnetism in the layered, ferromagnetic insulator CrI₃. *Chem. Mater.* **27**, 612–620 (2015). [doi:10.1021/cr504242t](https://doi.org/10.1021/cr504242t)
 7. M.-W. Lin, H. L. Zhuang, J. Yan, T. Z. Ward, A. A. Puzos, C. M. Rouleau, Z. Gai, L. Liang, V. Meunier, B. G. Sumpter, P. Ganesh, P. R. C. Kent, D. B. Geohegan, D. G. Mandrus, K. Xiao, Ultrathin nanosheets of CrSiTe₃: A semiconducting two-dimensional ferromagnetic material. *J. Mater. Chem. C Mater. Opt. Electron. Devices* **4**, 315–322 (2016). [doi:10.1039/C5TC03463A](https://doi.org/10.1039/C5TC03463A)
 8. Y. Tian, M. J. Gray, H. Ji, R. J. Cava, K. S. Burch, Magneto-elastic coupling in a potential ferromagnetic 2D atomic crystal. *2D Mater.* **3**, 025035 (2016). <https://doi.org/10.1088/2053-1583/3/2/025035>
 9. X. Wang, K. Du, Y. Y. F. Liu, P. Hu, J. Zhang, Q. Zhang, M. H. S. Owen, X. Lu, C. K. Gan, P. Sengupta, C. Kloc, Q. Xiong, Raman spectroscopy of atomically thin two-dimensional magnetic iron phosphorus trisulfide (FePS₃) crystals. *2D Mater.* **3**, 031009 (2016). <https://doi.org/10.1088/2053-1583/3/3/031009>
 10. J.-U. Lee, S. Lee, J. H. Ryoo, S. Kang, T. Y. Kim, P. Kim, C.-H. Park, J.-G. Park, H. Cheong, Ising-type magnetic ordering in atomically thin FePS₃. *Nano Lett.* **16**, 7433–7438 (2016). [doi:10.1021/acs.nanolett.6b03052](https://doi.org/10.1021/acs.nanolett.6b03052) [Medline](#)
 11. D. C. Worledge, T. H. Geballe, Magneto-resistive double spin filter tunnel junction. *J. Appl. Phys.* **88**, 5277–5279 (2000). [doi:10.1063/1.1315619](https://doi.org/10.1063/1.1315619)
 12. G.-X. Miao, M. Müller, J. S. Moodera, Magnetoresistance in double spin filter tunnel junctions with nonmagnetic electrodes and its unconventional bias dependence. *Phys. Rev. Lett.* **102**, 076601 (2009). [doi:10.1103/PhysRevLett.102.076601](https://doi.org/10.1103/PhysRevLett.102.076601) [Medline](#)
 13. M. N. Baibich, J. M. Broto, A. Fert, F. Nguyen Van Dau, F. Petroff, P. Etienne, G. Creuzet, A. Friederich, J. Chazelas, Giant magnetoresistance of (001)Fe/(001)Cr magnetic superlattices. *Phys. Rev. Lett.* **61**, 2472–2475 (1988). [doi:10.1103/PhysRevLett.61.2472](https://doi.org/10.1103/PhysRevLett.61.2472) [Medline](#)
 14. G. Binasch, P. Grünberg, F. Saurenbach, W. Zinn, Enhanced magnetoresistance in layered magnetic structures with antiferromagnetic interlayer exchange. *Phys. Rev. B* **39**, 4828–4830 (1989). [doi:10.1103/PhysRevB.39.4828](https://doi.org/10.1103/PhysRevB.39.4828) [Medline](#)
 15. B. Dieny, V. S. Speriosu, S. S. P. Parkin, B. A. Gurney, D. R. Wilhoit, D. Mauri, Giant magnetoresistive in soft ferromagnetic multilayers. *Phys. Rev. B* **43**, 1297–1300 (1991). [doi:10.1103/PhysRevB.43.1297](https://doi.org/10.1103/PhysRevB.43.1297) [Medline](#)
 16. M. Julliere, Tunneling between ferromagnetic films. *Phys. Lett. A* **54**, 225–226 (1975). [doi:10.1016/0375-9601\(75\)90174-7](https://doi.org/10.1016/0375-9601(75)90174-7)
 17. J. S. Moodera, L. R. Kinder, T. M. Wong, R. Meservey, Large magnetoresistance at room temperature in ferromagnetic thin film tunnel junctions. *Phys. Rev. Lett.* **74**, 3273–3276 (1995). [doi:10.1103/PhysRevLett.74.3273](https://doi.org/10.1103/PhysRevLett.74.3273) [Medline](#)
 18. T. Miyazaki, N. Tezuka, Giant magnetic tunneling effect in Fe/Al₂O₃/Fe junction. *J. Magn. Magn. Mater.* **139**, L231–L234 (1995). [doi:10.1016/0304-8853\(95\)90001-2](https://doi.org/10.1016/0304-8853(95)90001-2)
 19. S. Yuasa, T. Nagahama, A. Fukushima, Y. Suzuki, K. Ando, Giant room-temperature magnetoresistance in single-crystal Fe/MgO/Fe magnetic tunnel junctions. *Nat. Mater.* **3**, 868–871 (2004). [doi:10.1038/nmat1257](https://doi.org/10.1038/nmat1257) [Medline](#)
 20. S. S. P. Parkin, C. Kaiser, A. Panchula, P. M. Rice, B. Hughes, M. Samant, S.-H. Yang, Giant tunnelling magnetoresistance at room temperature with MgO (100) tunnel barriers. *Nat. Mater.* **3**, 862–867 (2004). [doi:10.1038/nmat1256](https://doi.org/10.1038/nmat1256) [Medline](#)
 21. S. Ikeda, J. Hayakawa, Y. Ashizawa, Y. M. Lee, K. Miura, H. Hasegawa, M. Tsunoda, F. Matsukura, H. Ohno, Tunnel magnetoresistance of 604% at 300 K by suppression of Ta diffusion in CoFeB/MgO/CoFeB pseudo-spin-valves annealed at high temperature. *Appl. Phys. Lett.* **93**, 082508 (2008). [doi:10.1063/1.2976435](https://doi.org/10.1063/1.2976435)
 22. L. Britnell, R. V. Gorbachev, R. Jalil, B. D. Belle, F. Schedin, A. Mishchenko, T. Georgiou, M. I. Katsnelson, L. Eaves, S. V. Morozov, N. M. R. Peres, J. Leist, A. K. Geim, K. S. Novoselov, L. A. Ponomarenko, Field-effect tunneling transistor based on vertical graphene heterostructures. *Science* **335**, 947–950 (2012). [doi:10.1126/science.1218461](https://doi.org/10.1126/science.1218461) [Medline](#)
 23. G.-H. Lee, Y.-J. Yu, C. Lee, C. Dean, K. L. Shepard, P. Kim, J. Hone, Electron tunneling through atomically flat and ultrathin hexagonal boron nitride. *Appl. Phys. Lett.* **99**, 243114 (2011). [doi:10.1063/1.3662043](https://doi.org/10.1063/1.3662043)
 24. T. Georgiou, R. Jalil, B. D. Belle, L. Britnell, R. V. Gorbachev, S. V. Morozov, Y.-J. Kim, A. Gholinia, S. J. Haigh, O. Makarovsky, L. Eaves, L. A. Ponomarenko, A. K. Geim, K. S. Novoselov, A. Mishchenko, Vertical field-effect transistor based on graphene-WS₂ heterostructures for flexible and transparent electronics. *Nat. Nanotechnol.* **8**, 100–103 (2013). [doi:10.1038/nnano.2012.224](https://doi.org/10.1038/nnano.2012.224) [Medline](#)
 25. A. Soumyanarayanan, N. Reyren, A. Fert, C. Panagopoulos, Emergent phenomena induced by spin-orbit coupling at surfaces and interfaces. *Nature* **539**, 509–517 (2016). [doi:10.1038/nature19820](https://doi.org/10.1038/nature19820) [Medline](#)
 26. S. A. Wolf, D. D. Awschalom, R. A. Buhrman, J. M. Daughton, S. von Molnár, M. L. Roukes, A. Y. Chtchelkanova, D. M. Treger, Spintronics: A spin-based electronics vision for the future. *Science* **294**, 1488–1495 (2001). [doi:10.1126/science.1065389](https://doi.org/10.1126/science.1065389) [Medline](#)
- <foot>27. See the supplementary materials.</foot>
28. T. R. McGuire, R. I. Potter, Anisotropic magnetoresistance in ferromagnetic 3D alloys. *IEEE Trans. Magn.* **11**, 1018–1038 (1975). [doi:10.1109/TMAG.1975.1058782](https://doi.org/10.1109/TMAG.1975.1058782)
 29. O. Hellwig, T. L. Kirk, J. B. Kortright, A. Berger, E. E. Fullerton, A new phase diagram for layered antiferromagnetic films. *Nat. Mater.* **2**, 112–116 (2003). [doi:10.1038/nmat806](https://doi.org/10.1038/nmat806) [Medline](#)
 30. O. Hellwig, A. Berger, E. E. Fullerton, Domain walls in antiferromagnetically coupled multilayer films. *Phys. Rev. Lett.* **91**, 197203 (2003). [doi:10.1103/PhysRevLett.91.197203](https://doi.org/10.1103/PhysRevLett.91.197203) [Medline](#)
 31. B. Chen, H. Xu, C. Ma, S. Mattauch, D. Lan, F. Jin, Z. Guo, S. Wan, P. Chen, G. Gao, F. Chen, Y. Su, W. Wu, All-oxide-based synthetic antiferromagnets exhibiting layer-resolved magnetization reversal. *Science* **357**, 191–194 (2017). [doi:10.1126/science.aak9717](https://doi.org/10.1126/science.aak9717) [Medline](#)
 32. M. Charilaou, C. Bordel, F. Hellman, Magnetization switching and inverted hysteresis in perpendicular antiferromagnetic superlattices. *Appl. Phys. Lett.* **104**, 212405 (2014). [doi:10.1063/1.4880821](https://doi.org/10.1063/1.4880821)
 33. D. C. Ralph, M. D. Stiles, Spin transfer torques. *J. Magn. Magn. Mater.* **320**, 1190–1216 (2008). [doi:10.1016/j.jmmm.2007.12.019](https://doi.org/10.1016/j.jmmm.2007.12.019)
 34. D. MacNeill, G. M. Stiehl, M. H. D. Guimarães, R. A. Buhrman, J. Park, D. C. Ralph, Control of spin-orbit torques through crystal symmetry in WTe₂/ferromagnet bilayers. *Nat. Phys.* **13**, 300–305 (2017). [doi:10.1038/nphys3933](https://doi.org/10.1038/nphys3933)
 35. P. Blake, E. W. Hill, A. H. Castro Neto, K. S. Novoselov, D. Jiang, R. Yang, T. J. Booth, A. K. Geim, Making graphene visible. *Appl. Phys. Lett.* **91**, 063124 (2007). [doi:10.1063/1.2768624](https://doi.org/10.1063/1.2768624)
 36. P. J. Zomer, M. H. D. Guimarães, J. C. Brant, N. Tombros, B. J. Van Wees, Fast pick up technique for high quality heterostructures of bilayer graphene and hexagonal boron nitride. *Appl. Phys. Lett.* **105**, 013101 (2014). [doi:10.1063/1.4886096](https://doi.org/10.1063/1.4886096)
 37. K. Sato, Measurement of magneto-optical Kerr effect using piezo-birefringent modulator. *Jpn. J. Appl. Phys.* **20**, 2403–2409 (1981). [doi:10.1143/JJAP.20.2403](https://doi.org/10.1143/JJAP.20.2403)
 38. R. R. Birss, *Symmetry and Magnetism* (Elsevier Science & Technology, Amsterdam, North-Holland, 1964).
 39. L. Onsager, Reciprocal relations in irreversible processes. I. *Phys. Rev.* **37**, 405–426 (1931). [doi:10.1103/PhysRev.37.405](https://doi.org/10.1103/PhysRev.37.405)

ACKNOWLEDGMENTS

We thank Yongtao Cui, Guoxing Miao, and Sara Majetich for insightful discussion. **Funding:** Work at the University of Washington was mainly supported by the Department of Energy, Basic Energy Sciences, Materials Sciences and Engineering Division (DE-SC0018171). Device fabrication and part of transport measurements are supported by NSF-DMR-1708419, NSF MRSEC 1719797, and UW Innovation Award. D.C.'s contribution is supported by DE-SC0002197. Work at CMU is supported by DOE BES DE-SC0012509. Work at HKU is supported by the Croucher Foundation (Croucher Innovation Award), UGC of HKSAR (AoE/P-04/08), and the HKU ORA. Work at ORNL (M.A.M.) was supported by the U.S.

Department of Energy, Office of Science, Basic Energy Sciences, Materials Sciences and Engineering Division. K.W. and T.T. acknowledge support from the Elemental Strategy Initiative conducted by the MEXT, Japan and JSPS KAKENHI Grant Numbers JP15K21722. D.X. acknowledges the support of a Cottrell Scholar Award. X.X. acknowledges the support from the State of Washington funded Clean Energy Institute and from the Boeing Distinguished Professorship in Physics. **Author contributions:** W.Y. and X.X. conceived the project. T.S. and X.C. fabricated the devices and performed the experiments, assisted by B.H., N.P.W., K.L.S., and L.Z., supervised by X.X., W.Y., D.X., and D.H.C. T.S. and X.X. analyzed the data, with theory support from M.T., W.Y., X.Z., and D.X. M.A.M. provided and characterized bulk CrI₃ crystals. T.T. and K.W. provided and characterized bulk hBN crystals. T.S., X.X., W.Y., D.X., and D.H.C. wrote the manuscript with input from all authors. **Competing interests:** None declared. **Data availability:** All data files are available from Harvard Dataverse at <https://doi.org/10.7910/DVN/TOTIWA>.

SUPPLEMENTARY MATERIALS

www.sciencemag.org/cgi/content/full/science.aar4851/DC1

Materials and Methods

Supplementary Text

Figs. S1 to S11

Table S1

References (35–39)

20 November 2017; accepted 24 April 2018

Published online 3 May 2018

10.1126/science.aar4851

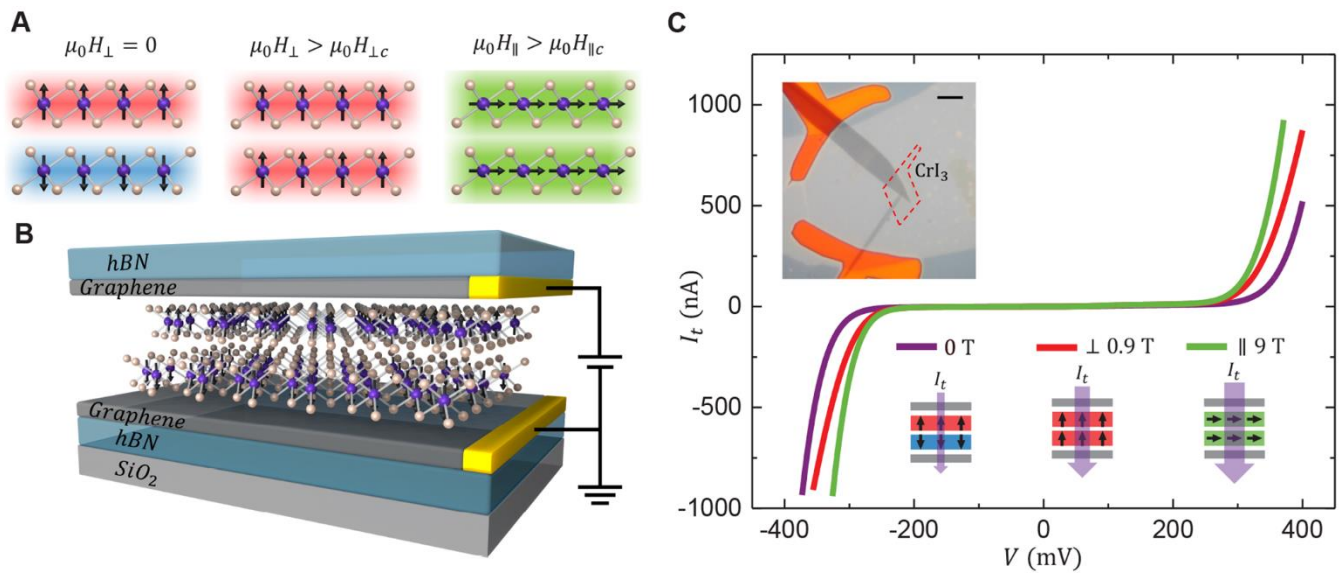


Fig. 1. Spin-filter effects in layered-antiferromagnetic CrI₃. (A) Schematic of magnetic states in bilayer CrI₃. Left: layered-antiferromagnetic state which suppresses the tunneling current at zero magnetic field; middle and right: fully spin-polarized states with out-of-plane and in-plane magnetizations, which do not suppress it. (B) Schematic of 2D spin-filter magnetic tunnel junction (sf-MTJ), with bilayer CrI₃ functioning as the spin-filter sandwiched between few-layer graphene contacts. (C) Tunneling current of a bilayer CrI₃ sf-MTJ at selected magnetic fields. Top inset: optical microscope image of the device (scale bar 5 μm). The red dashed line shows the position of the bilayer CrI₃. Bottom: schematic of the magnetic configuration for each I_t - V curve.

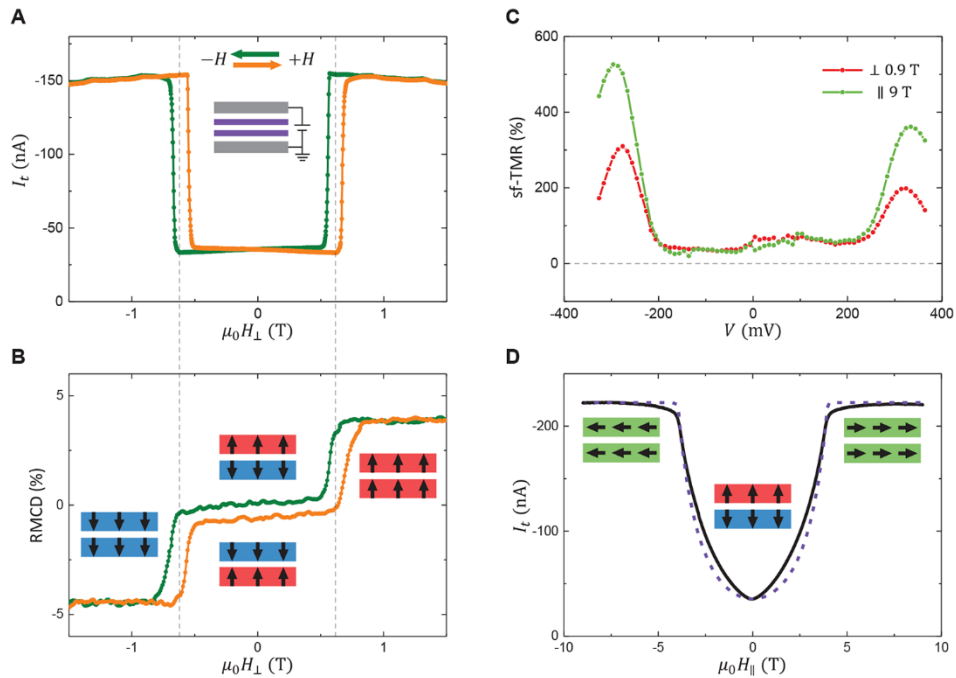


Fig. 2. Double spin-filter MTJ from bilayer CrI₃. (A) Tunneling current as a function of out-of-plane magnetic field ($\mu_0 H_{\perp}$) at a selected bias voltage (-290 mV). Green (orange) curve corresponds to decreasing (increasing) magnetic field. The junction area is about $0.75 \mu\text{m}^2$. (B) Reflective magnetic circular dichroism (RMCD) of the same device at zero bias. Insets show the corresponding magnetic states. (C) Extracted sf-TMR ratio as a function of bias based on the I_t - V curves in Fig. 1C. (D) Tunneling current as a function of in-plane magnetic field ($\mu_0 H_{\parallel}$) (black) at a selected bias voltage (-290 mV) with simulations (dashed purple). Insets show the corresponding magnetic states.

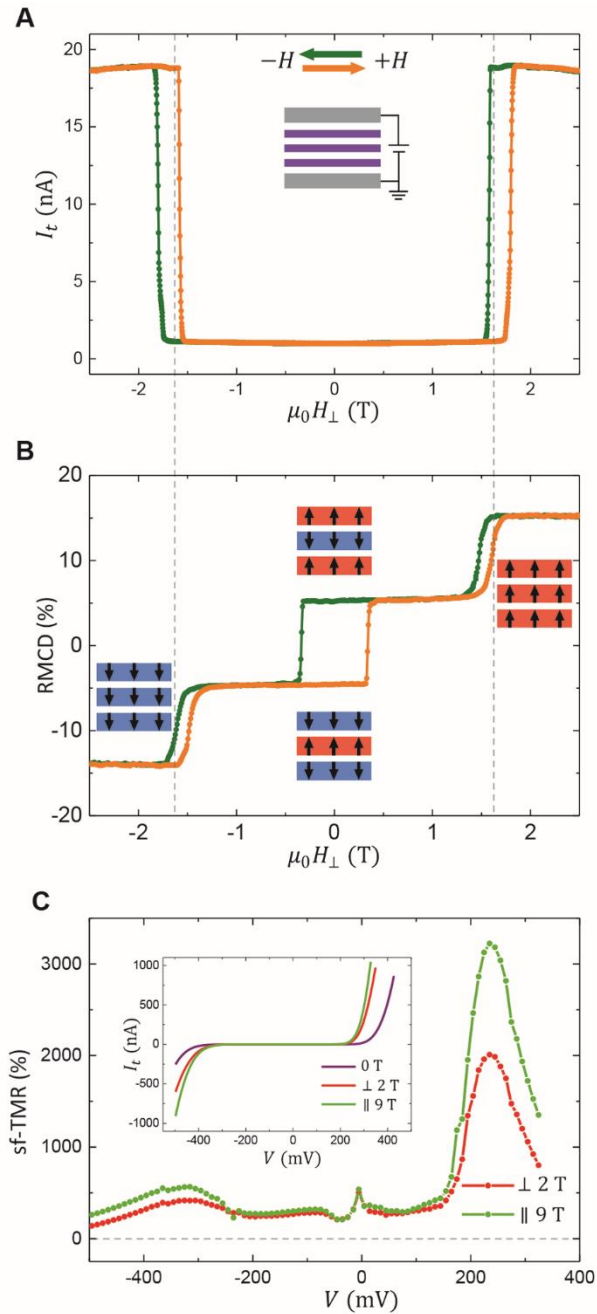


Fig. 3. Giant sf-TMR of a trilayer CrI₃ sf-MTJ. (A) Tunneling current as a function of out-of-plane magnetic field ($\mu_0 H_{\perp}$) at a selected bias voltage (235 mV). The junction area is about $0.06 \mu\text{m}^2$. (B) RMCD of the same device at zero bias showing antiferromagnetic interlayer coupling. Insets show the corresponding magnetic states. (C) sf-TMR ratio calculated from the I_t - V data shown in the inset.

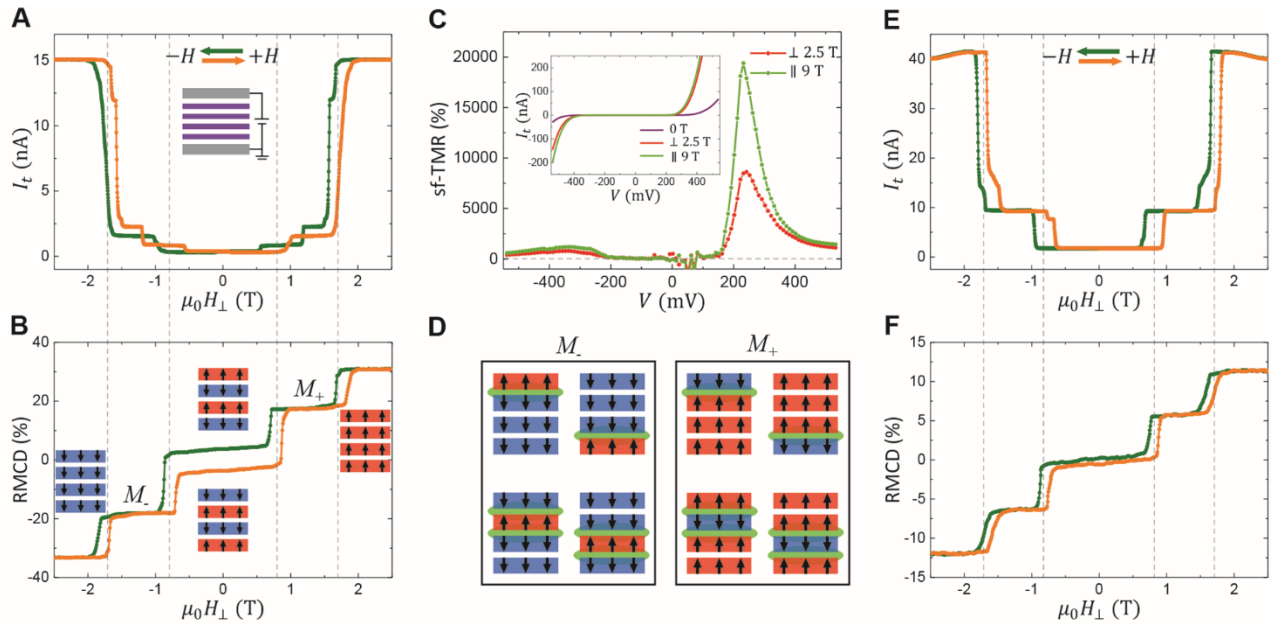


Fig. 4. Four-layer CrI₃ sf-MTJs with extraordinarily large sf-TMR and multiple resistance states. (A) Tunneling current as a function of out-of-plane magnetic field ($\mu_0 H_{\perp}$) at a selected bias voltage (300 mV), and (B) the corresponding RMCD of the same device at zero bias. Insets show the corresponding magnetic states. The junction area is about 2.2 μm^2 . (C) Calculated sf-TMR ratio as a function of bias based on the I_t - V curves in the inset. (D) Schematic of possible magnetic states corresponding to the intermediate plateaus in (A) and (B). Green lines show the current-blocking interfaces. (E) and (F) Tunneling current and RMCD from another four-layer CrI₃ sf-MTJ. The junction area is about 1.3 μm^2 .

Giant tunneling magnetoresistance in spin-filter van der Waals heterostructures

Tiancheng Song, Xinghan Cai, Matisse Wei-Yuan Tu, Xiaouo Zhang, Bevin Huang, Nathan P. Wilson, Kyle L. Seyler, Lin Zhu, Takashi Taniguchi, Kenji Watanabe, Michael A. McGuire, David H. Cobden, Di Xiao, Wang Yao and Xiaodong Xu

published online May 3, 2018

ARTICLE TOOLS

<http://science.sciencemag.org/content/early/2018/05/02/science.aar4851>

SUPPLEMENTARY MATERIALS

<http://science.sciencemag.org/content/suppl/2018/05/02/science.aar4851.DC1>

RELATED CONTENT

<http://science.sciencemag.org/content/sci/early/2018/05/02/science.aar3617.full>

REFERENCES

This article cites 37 articles, 5 of which you can access for free
<http://science.sciencemag.org/content/early/2018/05/02/science.aar4851#BIBL>

PERMISSIONS

<http://www.sciencemag.org/help/reprints-and-permissions>

Use of this article is subject to the [Terms of Service](#)